JACS
JOURNAL OF THE AMERICAN CHEMICAL SOCIETY

Article

pubs.acs.org/JACS

Impact of Shape Persistence on the Porosity of Molecular Cages

Timothy P. Moneypenny, II,[†] Nathan P. Walter,[‡] Zhikun Cai,[‡] Yu-Run Miao,[†] Danielle L. Gray,[§] Jordan J. Hinman,[†] Semin Lee,[∥] Yang Zhang,*[,‡,∥] and Jeffrey S. Moore*[,†,∥]

[†]Department of Chemistry, University of Illinois at Urbana—Champaign, Urbana, Illinois 61801, United States

[‡]Department of Nuclear, Plasma, and Radiological Engineering, University of Illinois at Urbana—Champaign, Urbana, Illinois 61801, United States

[§]School of Chemical Sciences, University of Illinois at Urbana—Champaign, Urbana, Illinois 61801, United States

[∥]Beckman Institute for Advanced Science and Technology, University of Illinois at Urbana—Champaign, Urbana, Illinois 61801, United States

Supporting Information

ABSTRACT: Porous materials provide a plethora of technologically important applications that encompass molecular separations, catalysis, and adsorption. The majority of research in this field involves network solids constructed from multitopic constituents that, when assembled either covalently or ionically, afford macromolecular arrangements with micro- or mesoporous apertures. Recently, porous solids fabricated from discrete organic cages have garnered much interest due to their ease of handling and solution processability. Although this class of materials is a promising alternative to network solids, fundamental studies are still required to elucidate critical structure–function relationships that govern microporosity. Here, we report a systematic investigation of the effects of building block shape-persistence on the porosity of molecular cages. Alkyne metathesis and edge-specific postsynthetic modifications afforded three organic cages with alkynyl, alkenyl, and alkyl edges, respectively. Nitrogen adsorption experiments conducted on rapidly crystallized and slowly crystallized solids illustrated a general trend in porosity: alkynyl > alkenyl > alkyl. To understand the molecular-scale origin of this trend, we investigated the short and long time scale molecular motions of the molecular cages using ab initio molecular dynamics (AIMD) and classical molecular dynamics (MD) simulations. Our combined experimental and computational results demonstrate that the microporosity of molecular cages directly correlates with shape persistence. These findings discern fundamental molecular requirements for rationally designing porous molecular solids.

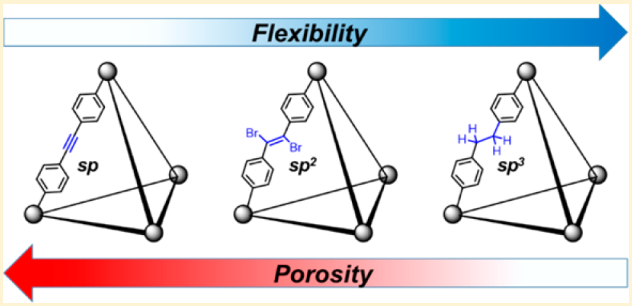

INTRODUCTION

The widespread interest in porous materials from both fundamental and technological perspectives has led to extensive applications including adsorption, catalysis, and molecular separation.[1] Three-dimensional extended network materials such as zeolites,[2,3] metal–organic frameworks (MOFs),[4−8] covalent organic frameworks (COFs),[9−12] and microporous network polymers[13−15] all contribute to the extensive literature on this topic and provide the bulk of current porous material technology. Recently, an emerging area of interest is the study of porous organic cages (POCs) and their solid-state molecular assemblies.[1,16−18] Pioneering research from the Mastalerz and Cooper groups demonstrate the potential for these molecules to exhibit unique pore topologies that are otherwise inaccessible with nonporous discrete molecules.[18−21] Additionally, unlike networks, which are generally insoluble and cumbersome to modify and manipulate, POCs are soluble in common organic solvents.[18] This provides the significant advantage of solution processability, which allows for ease of handling, film-deposition, cocrystallization of multiple components, and guest recognition.[1]

Although the field of POCs has seen many recent advances, fundamental studies relating molecular structure to macroscopic properties are needed to accelerate rational design. For example, current research efforts in the field of MOFs involve constructing frameworks with flexible building units that expand or "breathe" when exposed to adsorbates.[22−24] While flexibility in MOFs provides an avenue toward functional and responsive materials, introducing flexibility in POCs tends to induce adverse effects. Since most molecular cages possess windows resembling the size of small gas molecules (<2 nm), cage motion greatly affects the overall porosity of these materials.[25,26] Researchers have shown that cage flexibility permits cooperative diffusion mechanisms, whereby transient molecular reorganizations induced by the guest molecule provide accessible pathways for transport by diffusion.[25,26] However, if the cage molecule becomes too flexible, then removal of enclatherated solvent molecules from the crystal lattice is often accompanied by an overall collapse of the cage

Received: January 6, 2017
Published: February 3, 2017

DOI: 10.1021/jacs.7b00189
J. Am. Chem. Soc. 2017, 139, 3259−3264

itself, thus significantly reducing the adsorption capacity or eliminating it completely. For example, Zhang and co-workers reported flexible [2 + 3] amine cages that collapsed after desolvation to yield a material with very low porosity.[27] Mastalerz and co-workers synthesized [4 + 6] salicylbisimine cages that collapsed upon hydrogenation to the corresponding amines.[28] Cooper and co-workers reported a [4 + 6] imine cage that collapsed after reduction to amines, then reachieved shape persistence and porosity after postsynthetic tying with formaldehyde.[29]

Although these experiments hint at the undesirable effects of excess molecular flexibility, they describe all-or-nothing scenarios where added molecular freedom is met with complete cage collapse. To date, there have not been any studies investigating the effects of gradual alterations in flexibility on the porosity of molecular cages. Herein, we describe a system that specifically modifies the edges of a POC previously synthesized by our group, $\mathbf{Td_A}$ (Scheme 1),[30] to achieve

Scheme 1. Synthesis of $\mathbf{Td_H}$ and $\mathbf{Td_{Br}}$ from PSMs of $\mathbf{Td_A}$

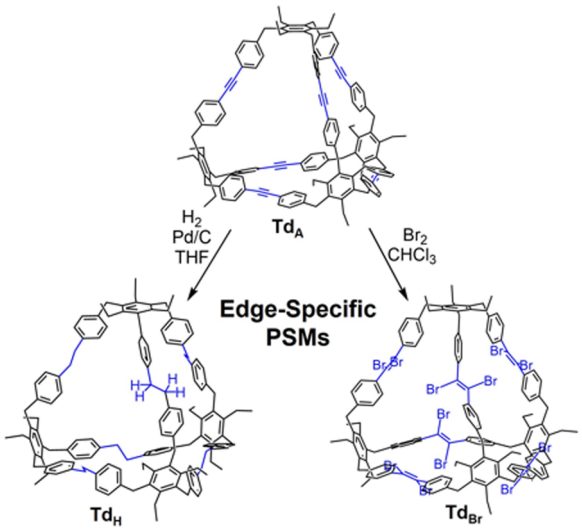

controlled, stepwise adjustments in flexibility. Utilizing alkyne metathesis (AM) and postsynthetic modifications (PSMs), we synthesized organic cages of varying molecular rigidity: $\mathbf{Td_A}$, $\mathbf{Td_{Br}}$, and $\mathbf{Td_H}$ (Scheme 1). X-ray crystal structures confirmed their tetrahedral geometry and transformations at all six edges. Nitrogen adsorption experiments of both rapidly crystallized and slowly crystallized samples exhibited a trend in surface area: $\mathbf{Td_A}$ > $\mathbf{Td_{Br}}$ > $\mathbf{Td_H}$. Short-time ab initio molecular dynamics (AIMD) and long-time classical molecular dynamics (MD) modeling of cage motions corroborated the trend in our experimental data and emphasized that shape-persistence governs the microporosity of these materials.

RESULTS AND DISSCUSSION

Cage Synthesis and Characterization. Recently, we reported the synthesis of $\mathbf{Td_A}$ utilizing AM, a powerful tool to synthesize aryleneethynylene-based molecular architectures such as macrocycles,[31,32] cages,[30,33,34] and frameworks.[35] As previously described,[30] a 1,3,5-tribenzyl-2,4,6-triethylbenzene vertex precursor with a well-defined, alternating up−down conformation afforded $\mathbf{Td_A}$ in nearly quantitative yields. The new modified cages, $\mathbf{Td_{Br}}$ and $\mathbf{Td_H}$, were synthesized from $\mathbf{Td_A}$ using PSMs in moderate to high yields. Specifically, $\mathbf{Td_{Br}}$ was synthesized in 40% yield in one step by bromination using excess bromine in chloroform ($CHCl_3$). The ^{1}H NMR reveals only two sets of aromatic doublets at 7.44 and 7.11 ppm, indicating exclusively one geometrical isomer of the dibromoalkene formed (Figure S5). The ^{13}C NMR spectrum confirms only one resonance at 118.11 ppm corresponding to a single dibromoalkenyl carbon (Figure S6), thus the PSM occurred stereoselectively. Additionally, $\mathbf{Td_H}$ was synthesized in 90% yield by hydrogenation of $\mathbf{Td_A}$ using Pd/C and hydrogen gas in tetrahydrofuran (THF). ^{1}H NMR reveals a new proton resonance at 2.79 ppm, indicating the presence of benzylic protons (Figure S3). ^{13}C NMR reveals the expected benzylic carbon resonance at 39.0 ppm (Figure S4).

Single Crystal XRD Analysis. To compare their solid-state packing and confirm transformation of all six alkynyl edges, we performed single crystal X-ray diffraction analysis (Figure 1). Cage $\mathbf{Td_A}$ crystallized from slow diffusion of a 1:1 (v/v) layered mixture of $CHCl_3$ and toluene in the tetragonal space group $I4_1/a$.[30] The cages pack in an edge-to-edge fashion exhibiting mainly CH···π (alkyne) interactions. Cage $\mathbf{Td_{Br}}$ crystallized from slow diffusion of a 1:1 (v/v) mixture of $CHCl_3$ and toluene in the monoclinic space group $C2/c$. The tetrahedral structure remained intact, and all six alkynyl linkages were transformed exclusively to the corresponding *trans*-dibromoalkene. We hypothesize that rigidity enforced by cage vertices restricts edge motion, prompting solely the trans geometric isomer to form. A similar result was observed with postsynthetic bromination of a MOF.[36] The $\mathbf{Td_{Br}}$ cages align primarily in edge-to-edge motifs through CH···Br interactions. Cage $\mathbf{Td_H}$ crystallized from slow diffusion of a 1:1 (v/v) layered mixture of $CHCl_3$ and methanol in the trigonal $R\bar{3}$ space group. The tetrahedral structure remained intact and all six alkynyl linkages transformed to the corresponding alkyl carbon atoms. The resulting crystal is a racemate of two atropisomers (M and P, depicted as blue and orange respectively in Figure 1) that pack in both window-to-window and edge-to-edge motifs through T-shaped CH···π (aryl) interactions.

Preparation of Solids. As reported by Cooper and co-workers, the preparative conditions for molecular cages greatly influence the porosity of the resulting material.[18,37] In light of their findings, we prepared cage solids using two procedures: rapid and slow crystallization. Rapidly crystallized powders were prepared by precipitation from a $CHCl_3$ solution with the rapid addition of an excess amount of methanol. The mixtures were stirred for 30 min, filtered, and dried under high vacuum for 12 h. Powder X-ray diffraction (PXRD) confirmed that these samples have low crystallinity (Figures S18−S20) owing to the presence of broad, poorly defined diffraction peaks. Scanning electron microscopy (Figure 2a−c) showed that each powder exhibits its own unique morphology. Investigation of how the rate of precipitation affects the topology and gas uptake of these powders will be addressed in future studies.

Slowly crystallized samples of each cage were prepared by slow evaporation of a $CHCl_3$ solution over the course of 5−7 days. The solids were desolvated by leaving the samples open to air for 12 h, then dried under high vacuum for 1 h. PXRD of the desolvated crystals of $\mathbf{Td_A}$ and $\mathbf{Td_{Br}}$ exhibited broad peaks, indicating the loss of crystallinity and/or reduction of crystallite size as a result of removing enclatherated solvent (Figures S18 and S19). SEM images of $\mathbf{Td_A}$ and $\mathbf{Td_{Br}}$ desolvated crystals revealed that these solids exhibit significant cracking and breaking (Figure 2e,f). Interestingly, the PXRD pattern of $\mathbf{Td_H}$ showed almost no distinguishable diffraction peaks, indicating

DOI: 10.1021/jacs.7b00189
J. Am. Chem. Soc. 2017, 139, 3259−3264

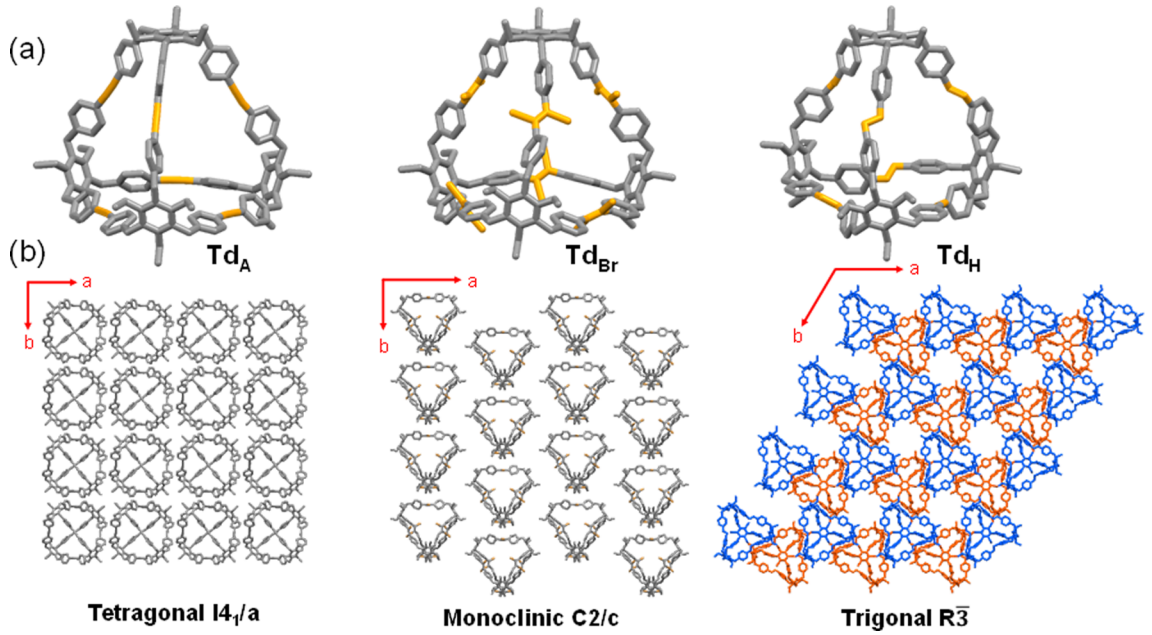

Figure 1. (a) X-ray crystal structures of $\mathbf{Td_A}$, $\mathbf{Td_{Br}}$, and $\mathbf{Td_H}$ with hydrogens omitted for clarity. (b) Crystal packing viewed along the *c*-axis for $\mathbf{Td_A}$ and $\mathbf{Td_H}$ and the *c*′-axis for $\mathbf{Td_{Br}}$. Blue and orange cages correspond to atropisomers *M* and *P*, respectively.

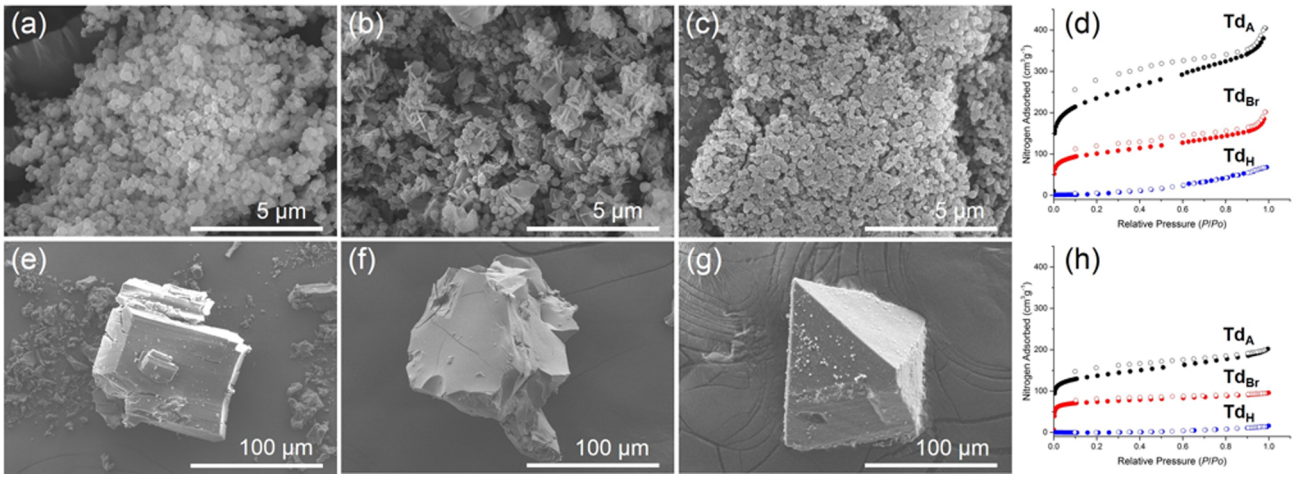

Figure 2. Scanning electron microscopy (SEM) images of prepared molecular cage solids. (a–c) Rapidly crystallized solids of $\mathbf{Td_A}$, $\mathbf{Td_{Br}}$, and $\mathbf{Td_H}$, respectively. (d) Gas adsorption isotherms of rapidly crystallized solids. (e–g) Slowly crystallized solids of $\mathbf{Td_A}$, $\mathbf{Td_{Br}}$, and $\mathbf{Td_H}$, respectively. (h) Gas adsorption isotherms of slowly crystallized solids.

that the sample had undergone a phase change to an amorphous solid (Figure S20). This phenomenon is indicative of cage collapse after removing enclatherated solvent.[29] We acknowledge that using different crystallization conditions may afford other polymorphs.

Nitrogen Adsorption Experiments. All samples were tested for nitrogen adsorption capacity by first outgassing and heating to 70 °C under high vacuum for 12 h before measuring the adsorption of nitrogen at 77 K. For each, a type I isotherm was observed, typical of microporous materials (Figure 2d,h).[38] The results of these experiments are summarized in Table 1. $\mathbf{Td_A}$ was the most porous, $\mathbf{Td_{Br}}$ showed intermediate porosity, and $\mathbf{Td_H}$ cage proved to be nonporous in both preparative conditions. It is interesting to note that the isotherms for $\mathbf{Td_A}$ and $\mathbf{Td_{Br}}$ exhibit adsorption hysteresis. While the exhibited hysteresis suggests some mesoporous character, this phenomenon cannot be justified by the crystal structures of these cages.

Table 1. Specific Surface Area Data of All Samples from Nitrogen Adsorption Experiments

powder	SA_{BET} (m^2g^{-1})	$SA_{Langmuir}$ (m^2g^{-1})	crystal	SA_{BET} (m^2g^{-1})	$SA_{Langmuir}$ (m^2g^{-1})
$\mathbf{Td_A}$	823	941	$\mathbf{Td_A}$	509	586
$\mathbf{Td_{Br}}$	378	436	$\mathbf{Td_{Br}}$	279	319
$\mathbf{Td_H}$	5	6	$\mathbf{Td_H}$	0	0

However, as stated earlier, both $\mathbf{Td_A}$ and $\mathbf{Td_{Br}}$ crystals exhibit significant cracking after desolvation due to the strong interactions between the cages and solvent molecules. Fracturing of cage crystals can induce mesoporous character during desorption and thus give rise to hysteresis, as previously reported.[19] A similar argument holds true for cage powders in this case, as rapid precipitation results in large crystal defects in the bulk material.[19]

DOI: 10.1021/jacs.7b00189
J. Am. Chem. Soc. 2017, 139, 3259–3264

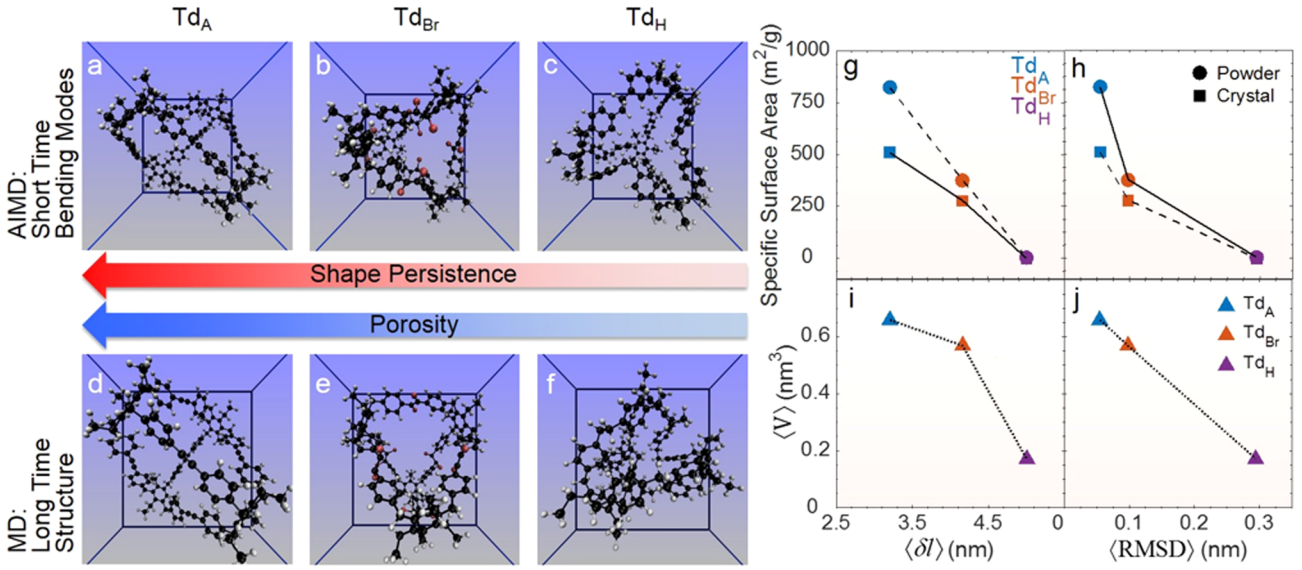

Figure 3. (a–c) Molecular configurations of $\mathbf{Td_A}$, $\mathbf{Td_{Br}}$, and $\mathbf{Td_H}$ at their maximum concave bending from AIMD simulations. (d–f) Long-time configurations from classical MD simulations. (g–j) Quantitative measures of porosity and volume plotted against measures of flexibility. All lines are included for guidance only.

Molecular Dynamics Simulations. To better understand the observed trend in the nitrogen adsorption experiments, we turned to theoretical computations. Our approach focused on modeling the molecular motion of individual cages on the picosecond time scale via AIMD and classical MD. AIMD and classical MD were performed to capture the short-time and long-time properties of the molecular cages, respectively, with initial configurations generated from X-ray coordinates. Figure 3 summarizes the main observations and quantities obtained from these simulations.

To quantify the short-time shape-persistence of cage building blocks, we performed AIMD simulations at 300 K in an NVT ensemble with a time step of 1 fs. The bending flexibility of the edges can be visually recognized from the simulation movies (Movies S1–S6). Cage $\mathbf{Td_A}$ shows the smallest amplitude of edge movement, while $\mathbf{Td_H}$ shows the largest. To be more precise, we computed the averaged deviation of each edge from its initial linear configuration, $\langle \delta l \rangle$, and used it to quantify the short-time flexibility of the edges. Figure 3a–c shows the maximal concave bending configuration of the edges of each molecular cages. Over an elapsed time period of 3 ps, the time-averaged edge deviations of $\mathbf{Td_A}$, $\mathbf{Td_{Br}}$, and $\mathbf{Td_H}$ were 3.2, 4.2, and 5.0 nm, respectively. These values correlate well with the experimentally measured specific surface area SA_{BET} values for both the powders and desolvated crystals (Figure 3g).

The long-time shape-persistence and volume/porosity of the molecular cages were modeled by classical MD simulations using the universal force field[39] with time steps of 0.05 fs for $\mathbf{Td_A}$ and 1.0 fs for $\mathbf{Td_{Br}}$ and $\mathbf{Td_H}$. Production runs were performed for 300 ps in an NVT ensemble at 300 K. We computed the time-averaged root mean squared deviation, ⟨RMSD⟩, of the molecular cages relative to their initial configurations, and used it to indicate the long-time flexibility of the entire molecule. Figure 3d–f shows the typical long-time structure of each molecular cage. Again, $\mathbf{Td_A}$ proved to be the most rigid structure with a ⟨RMSD⟩ of 0.05 nm, while $\mathbf{Td_{Br}}$ and $\mathbf{Td_H}$ had ⟨RMSD⟩ values of 0.1 and 0.3 nm, respectively. These values also correlate well with the experimentally measured specific area SA_{BET} values for both the powders and desolvated crystals (Figure 3h).

The time-averaged internal volume of molecular cage, $\langle V \rangle$, obtained from the classical MD simulations served as a theoretical indicator of the cage porosity. $\langle V \rangle$ was computed as the summation of volumes of many small internal tetrahedrons, which are constructed by connecting representative atoms on the edges of the original molecular cage (Figure S34). $\langle V \rangle$ correlates well with $\langle \delta l \rangle$ obtained from the AIMD simulation and with ⟨RMSD⟩ obtained from the classical MD simulation (Figure 3i,j). As an extreme example, the classical MD simulation was able to capture the partial collapse of $\mathbf{Td_H}$ during the simulation time window (Figure 3f), while $\mathbf{Td_A}$ and $\mathbf{Td_{Br}}$ retained their structure during the entire simulation. These results provide a molecular-scale understanding of the nonporous nature of desolvated $\mathbf{Td_H}$ solid, as well as its structural change to an amorphous solid after desolvation.

These simulations suggest that shape-persistence of the molecular cages governs their porosity. Close inspection of cage motion in the simulation movies reveals key structural features responsible for this phenomenon. In the simulations for $\mathbf{Td_A}$, the alkynyl edges restrict bending and/or rotation about the $C_{arene}—C_{alkynyl}—C_{alkynyl}—C_{arene}$ torsional angle. This restricted movement fortifies the vertices and prevents partial window closure and cage collapse after desolvation. In the simulations for $\mathbf{Td_{Br}}$, the alkenyl edges provide limited bending and rotation about the $C_{arene}—C_{alkenyl}—C_{alkenyl}—C_{arene}$ torsional angle. This added flexibility allows the edges to bend in and out, which leads to partial blockage of cage windows in the process. However, the edges are still rigid enough to prevent the vertices from folding in. Finally, the simulations for $\mathbf{Td_H}$ indicate that the alkyl edges have essentially unrestricted bending and/or rotation about the $C_{arene}—C_{alkyl}—C_{alkyl}—C_{arene}$ torsion angle, which provides enough flexibility to allow at least two edges to collapse inward. Thus, the edges in $\mathbf{Td_H}$ are not rigid enough to maintain cage shape-persistence after desolvation.

Overall, although both $\mathbf{Td_A}$ and $\mathbf{Td_{Br}}$ retain their shape throughout the simulation (i.e., they maintain at least 95% of their initial volume), $\mathbf{Td_H}$ collapses, preserving only 10% of its

DOI: 10.1021/jacs.7b00189
J. Am. Chem. Soc. 2017, 139, 3259–3264

initial volume after tens of picoseconds. This loss in shape-persistence afforded nonporous molecular solids of $\mathbf{Td}_{\mathbf{H}}$ in both preparative conditions. In terms of the flexibility, our simulations indicate that even a minor increase in $\langle \delta l \rangle$ of 1.0 nm (from $\mathbf{Td}_{\mathbf{A}}$ to $\mathbf{Td}_{\mathbf{Br}}$) leads to a decrease in surface area of ca. 45% in desolvated crystals and ca. 54% in powders. Furthermore, an increase by 1.8 nm (from $\mathbf{Td}_{\mathbf{A}}$ to $\mathbf{Td}_{\mathbf{H}}$) leads to cage collapse and loss of porosity. The method presented here constitutes a qualitative analysis of the relationship between shape persistence and porosity. Certainly, other factors such as guest−host interactions may also contribute significantly to molecular flexibility and porosity, as previously reported.[40] However, the advantage of our method is that it requires significantly less computational power and provides a "fingerprint" of a given molecule independent of a specific guest.

CONCLUSIONS

We performed a systematic study of the effects of molecular shape-persistence on the porosity of molecular cage solids. Utilizing the significant advantage of cage solubility allowed us to modify $\mathbf{Td}_{\mathbf{A}}$ in high yields using PSMs with common organic reagents to afford $\mathbf{Td}_{\mathbf{Br}}$ and $\mathbf{Td}_{\mathbf{H}}$. These modifications characteristically affected their gas adsorption capacity and revealed a relationship between shape-persistence and porosity in both rapidly and slowly crystallized samples. AIMD and classical MD provided molecular-scale understanding of how bond flexibility affects porosity of the molecular cages and supported our experimental data.

While our single molecule simulations do not provide a quantitative prediction of transport properties and gas diffusion mechanisms in the bulk material, this approach exemplifies how minor changes in molecular design greatly affect the physical properties of the bulk. Our integrated synthetic and computational approach demonstrates that the microporosity of this class of molecular cage solids can be controlled through fine-tuning at both the atomic level by synthetic modifications and the microscale by modular molecular packing. Our high-throughput computational methodology, accompanied by powerful in silico materials design strategies,[41] may provide a route to screen potential candidate POCs before they are synthesized, eliminating trial-and-error practices. The ability to control and predict micro- and meso-porosity through modular assembly of rationally constructed building blocks unlocks the potential of designing porous materials with specific physical properties a priori. In effect, these results will help streamline the process of designing novel molecular architectures for targeted materials applications.

ASSOCIATED CONTENT

Supporting Information

The Supporting Information is available free of charge on the ACS Publications website at DOI: 10.1021/jacs.7b00189.

Simulation movie (MPG)
Simulation movie (MPG)
Simulation movie (MPG)
Simulation movie (MPG)
Simulation movie (MPG)
Simulation movie (MPG)
Single crystal crystallographic data, deposition number CCDC 1452245 ($\mathbf{Td}_{\mathbf{A}}$) (CIF)
Single crystal crystallographic data, deposition number CCDC 1504099 ($\mathbf{Td}_{\mathbf{Br}}$) (CIF)
Single crystal crystallographic data, deposition number CCDC 1504097 ($\mathbf{Td}_{\mathbf{H}}$) (CIF)
Experimental conditions and procedures, syntheses and compound characterizations including ^{1}H NMR, ^{13}C NMR, mass spectrometry data, PXRD, TGA, SEM images, simulation protocols, and additional references (PDF)

AUTHOR INFORMATION

Corresponding Authors

*zhyang@illinois.edu
*jsmoore@illinois.edu

ORCID

Timothy P. Moneypenny II: 0000-0001-8881-1518
Danielle L. Gray: 0000-0003-0059-2096
Semin Lee: 0000-0003-0873-9507
Jeffrey S. Moore: 0000-0001-5841-6269

Notes

The authors declare no competing financial interest.

ACKNOWLEDGMENTS

This work was supported by the National Science Foundation CHE under Grant Number 16-10328, by the U.S. Department of Energy, Office of Science, Office of Basic Energy Sciences, Materials Sciences and Engineering Division, under Award Number DE-SC-0014804, the National Science Foundation DMR under Grant Number 12-06355, and the U.S. Navy MURI under Grant Number N000141210828. S.L. gratefully acknowledges the Arnold and Mabel Beckman Foundation for a Beckman Institute Postdoctoral Fellowship. The authors would like to thank the School of Chemical Sciences NMR Lab and Mass Spectrometry Lab, the Center for Microanalysis of Materials at the Materials Research Laboratory, and the George L. Clark X-ray Facility and 3M Materials Laboratory. Crystallographic data of $\mathbf{Td}_{\mathbf{A}}$ was collected through the SCrALS (Service Crystallography at the Advanced Light Source) program at Beamline 11.3.1 at the Advanced Light Source (ALS), Lawrence Berkeley National Laboratory. The Advanced Light Source is supported by the Director, Office of Science, Office of Basic Energy Sciences, of the U.S. Department of Energy under contract No. DE-AC02-05CH11231.

REFERENCES

(1) Slater, A. G.; Cooper, A. I. *Science* **2015**, *348*, 988.
(2) Cheetham, A. K.; Férey, G.; Loiseau, T. *Angew. Chem., Int. Ed.* **1999**, *38*, 3268.
(3) Cundy, C. S.; Cox, P. A. *Chem. Rev.* **2003**, *103*, 663.
(4) Furukawa, H.; Cordova, K. E.; O'Keeffe, M.; Yaghi, O. M. *Science* **2013**, *341*, 1230444.
(5) Furukawa, H.; Ko, N.; Go, Y. B.; Aratani, N.; Choi, S. B.; Choi, E.; Yazaydin, A. O.; Snurr, R. Q.; O'Keeffe, M.; Kim, J.; Yaghi, O. M. *Science* **2010**, *329*, 424.
(6) Deng, H.; Olson, M. A.; Stoddart, J. F.; Yaghi, O. M. *Nat. Chem.* **2010**, *2*, 439.
(7) Eddaoudi, M.; Kim, J.; Rosi, N.; Vodak, D.; Wachter, J.; O'Keeffe, M.; Yaghi, O. M. *Science* **2002**, *295*, 469.
(8) Kitagawa, S.; Kitaura, R.; Noro, S.-i. *Angew. Chem., Int. Ed.* **2004**, *43*, 2334.
(9) Côté, A. P.; Benin, A. I.; Ockwig, N. W.; O'Keeffe, M.; Matzger, A. J.; Yaghi, O. M. *Science* **2005**, *310*, 1166.

DOI: 10.1021/jacs.7b00189
J. Am. Chem. Soc. 2017, 139, 3259−3264

(10) Côté, A. P.; El-Kaderi, H. M.; Furukawa, H.; Hunt, J. R.; Yaghi, O. M. *J. Am. Chem. Soc.* **2007**, *129*, 12914.
(11) Ding, S.-Y.; Wang, W. *Chem. Soc. Rev.* **2013**, *42*, 548.
(12) Segura, J. L.; Mancheno, M. J.; Zamora, F. *Chem. Soc. Rev.* **2016**, *45*, 5635−5671.
(13) Jiang, J.-X.; Su, F.; Trewin, A.; Wood, C. D.; Campbell, N. L.; Niu, H.; Dickinson, C.; Ganin, A. Y.; Rosseinsky, M. J.; Khimyak, Y. Z.; Cooper, A. I. *Angew. Chem., Int. Ed.* **2007**, *46*, 8574.
(14) McKeown, N. B.; Budd, P. M. *Macromolecules* **2010**, *43*, 5163.
(15) Vilela, F.; Zhang, K.; Antonietti, M. *Energy Environ. Sci.* **2012**, *5*, 7819.
(16) Mastalerz, M. *Chem. - Eur. J.* **2012**, *18*, 10082.
(17) Holst, J. R.; Trewin, A.; Cooper, A. I. *Nat. Chem.* **2010**, *2*, 915.
(18) Tozawa, T.; Jones, J. T. A.; Swamy, S. I.; Jiang, S.; Adams, D. J.; Shakespeare, S.; Clowes, R.; Bradshaw, D.; Hasell, T.; Chong, S. Y.; Tang, C.; Thompson, S.; Parker, J.; Trewin, A.; Bacsa, J.; Slawin, A. M. Z.; Steiner, A.; Cooper, A. I. *Nat. Mater.* **2009**, *8*, 973.
(19) Hasell, T.; Culshaw, J. L.; Chong, S. Y.; Schmidtmann, M.; Little, M. A.; Jelfs, K. E.; Pyzer-Knapp, E. O.; Shepherd, H.; Adams, D. J.; Day, G. M.; Cooper, A. I. *J. Am. Chem. Soc.* **2014**, *136*, 1438.
(20) Zhang, G.; Presly, O.; White, F.; Oppel, I. M.; Mastalerz, M. *Angew. Chem., Int. Ed.* **2014**, *53*, 1516.
(21) Jones, J. T. A.; Holden, D.; Mitra, T.; Hasell, T.; Adams, D. J.; Jelfs, K. E.; Trewin, A.; Willock, D. J.; Day, G. M.; Bacsa, J.; Steiner, A.; Cooper, A. I. *Angew. Chem., Int. Ed.* **2011**, *50*, 749.
(22) Linder-Patton, O. M.; Bloch, W. M.; Coghlan, C. J.; Sumida, K.; Kitagawa, S.; Furukawa, S.; Doonan, C. J.; Sumby, C. J. *CrystEngComm* **2016**, *18*, 4172.
(23) Li, L.; Krishna, R.; Wang, Y.; Yang, J.; Wang, X.; Li, J. *J. Mater. Chem. A* **2016**, *4*, 751.
(24) Hyun, S.-m.; Lee, J. H.; Jung, G. Y.; Kim, Y. K.; Kim, T. K.; Jeoung, S.; Kwak, S. K.; Moon, D.; Moon, H. R. *Inorg. Chem.* **2016**, *55*, 1920.
(25) Jiang, S.; Jelfs, K. E.; Holden, D.; Hasell, T.; Chong, S. Y.; Haranczyk, M.; Trewin, A.; Cooper, A. I. *J. Am. Chem. Soc.* **2013**, *135*, 17818.
(26) Holden, D.; Jelfs, K. E.; Trewin, A.; Willock, D. J.; Haranczyk, M.; Cooper, A. I. *J. Phys. Chem. C* **2014**, *118*, 12734.
(27) Jin, Y.; Voss, B. A.; Jin, A.; Long, H.; Noble, R. D.; Zhang, W. *J. Am. Chem. Soc.* **2011**, *133*, 6650.
(28) Mastalerz, M.; Schneider, M. W.; Oppel, I. M.; Presly, O. *Angew. Chem., Int. Ed.* **2011**, *50*, 1046.
(29) Liu, M.; Little, M. A.; Jelfs, K. E.; Jones, J. T. A.; Schmidtmann, M.; Chong, S. Y.; Hasell, T.; Cooper, A. I. *J. Am. Chem. Soc.* **2014**, *136*, 7583.
(30) Lee, S.; Yang, A.; Moneypenny, T. P.; Moore, J. S. *J. Am. Chem. Soc.* **2016**, *138*, 2182.
(31) Sisco, S. W.; Larson, B. M.; Moore, J. S. *Macromolecules* **2014**, *47*, 3829.
(32) Li, L.; Che, Y.; Gross, D. E.; Huang, H.; Moore, J. S.; Zang, L. *ACS Macro Lett.* **2012**, *1*, 1335.
(33) Wang, Q.; Yu, C.; Long, H.; Du, Y.; Jin, Y.; Zhang, W. *Angew. Chem., Int. Ed.* **2015**, *54*, 7550.
(34) Wang, Q.; Zhang, C.; Noll, B. C.; Long, H.; Jin, Y.; Zhang, W. *Angew. Chem., Int. Ed.* **2014**, *53*, 10663.
(35) Zhu, Y.; Yang, H.; Jin, Y.; Zhang, W. *Chem. Mater.* **2013**, *25*, 3718.
(36) Marshall, R. J.; Griffin, S. L.; Wilson, C.; Forgan, R. S. *J. Am. Chem. Soc.* **2015**, *137*, 9527.
(37) Jiang, S.; Jones, J. T. A.; Hasell, T.; Blythe, C. E.; Adams, D. J.; Trewin, A.; Cooper, A. I. *Nat. Commun.* **2011**, *2*, 207.
(38) Sing, K. S. W.; Everett, D. H.; Haul, R. A. W.; Moscou, L.; Pierotti, R. A.; Rouquerol, J.; Siemieniewska, T. *Pure Appl. Chem.* **1985**, *57*, 603.
(39) Rappe, A. K.; Casewit, C. J.; Colwell, K. S.; Goddard, W. A.; Skiff, W. M. *J. Am. Chem. Soc.* **1992**, *114*, 10024.
(40) Manurung, R.; Holden, D.; Miklitz, M.; Chen, L.; Hasell, T.; Chong, S. Y.; Haranczyk, M.; Cooper, A. I.; Jelfs, K. E. *J. Phys. Chem. C* **2015**, *119*, 22577−22586.
(41) Jones, J. T. A.; Hasell, T.; Wu, X.; Bacsa, J.; Jelfs, K. E.; Schmidtmann, M.; Chong, S. Y.; Adams, D. J.; Trewin, A.; Schiffman, F.; Cora, F.; Slater, B.; Steiner, A.; Day, G. M.; Cooper, A. I. *Nature* **2011**, *474*, 367−371.

DOI: 10.1021/jacs.7b00189
J. Am. Chem. Soc. 2017, 139, 3259−3264